Pharm Res (2010) 27:1367–1376
DOI 10.1007/s11095-010-0128-4

RESEARCH PAPER

Particle Aerosolisation and Break-up in Dry Powder Inhalers 1: Evaluation and Modelling of Venturi Effects for Agglomerated Systems

William Wong • David F. Fletcher • Daniela Traini • Hak-Kim Chan • John Crapper • Paul M. Young

Received: 8 January 2010 / Accepted: 22 March 2010 / Published online: 6 April 2010

ABSTRACT

Purpose This study utilized a combination of computational fluid dynamics (CFD) and standardized entrainment tubes to investigate the influence of turbulence on the break-up and aerosol performance of a model inhalation formulation.

Methods Agglomerates (642.8 μm mean diameter) containing 3.91 μm median diameter primary spherical mannitol particles were prepared by spheronisation. A series of entrainment tubes with different Venturi sections were constructed *in silico*, and the flow pattern and turbulence/impaction parameters were predicted using CFD. The entrainment models were constructed from the *in silico* model using three-dimensional printing. The aerosol performance of the mannitol was assessed by entraining the agglomerates into the experimental tubes at a series of flow rates and assessing the size distribution downstream of the venturi via in-line laser diffraction.

Results A series of parameters (including Reynolds number (Re), turbulence kinetic energy, turbulence eddy frequency, turbulence length-scale, velocity and pressure drop) were calculated from the CFD simulation. The venturi diameter and volumetric flow rate were varied systematically. The particle size data of the agglomerated powders were then correlated with the CFD measurements. No correlation between turbulence and aerosol performance could be made (i.e. at a Reynolds number of 8,570, the $d_{0.1}$ was 52.5 μm ± 19.7 μm, yet at a Reynolds number of 12,000, the $d_{0.1}$ was 429.1 μm ± 14.8 μm). Lagrangian particle tracking indicated an increase in the number of impactions and the normal velocity component at the wall, with increased volumetric airflow and reduced venturi diameter. Chemical analysis of the mannitol deposited on the walls showed a linear relationship with respect to the theoretical number of impactions ($R^2 = 0.9620$). Analysis of the relationship between the CFD results and the experimental size data indicated a critical impact velocity was required to initiate agglomerate break-up (~0.4 $m.s^{-1}$).

Conclusion While this study focussed on the effect of turbulence on agglomerate break-up, the small amount of impaction, which inevitably occurs in the venturi assembly, appeared to dominate agglomerate break-up in this dry powder system.

KEY WORDS aerosolisation · agglomerate · CFD · DPI entrainment tubes · dry powder inhaler · turbulence · venturi

W. Wong • D. Traini • H.-K. Chan • P. M. Young (✉)
Advanced Drug Delivery Group, Faculty of Pharmacy,
University of Sydney,
Sydney, NSW 2006, Australia
e-mail: py@pharm.usyd.edu.au

D. F. Fletcher
School of Chemical and Biomolecular Engineering,
University of Sydney,
Sydney, NSW 2006, Australia

J. Crapper
Pharmaxis Ltd.,
Unit 2, 10 Rodborough Rd, Frenchs Forest,
Sydney, NSW 2086, Australia

INTRODUCTION

There are many dry powder inhaler (DPI) devices on the market, with the majority using either turbulence or particle-particle/particle-wall impaction to aerosolise the active pharmaceutical ingredient (API) (1–3). However, limited research has been conducted to elucidate the exact mechanism of aerosolisation and particle de-agglomeration in these systems. Historically, de-agglomeration rigs have been utilised to assess the mechanism of powder break-up at the fundamental level (4). Many of these previous studies

have been cross-disciplinary (for example in the printing or minerals industry), and the rig designs diverse. Essentially, the apparatuses have been generally based on entrainment tube designs with incorporated impaction or turbulence-promoting features (4).

In terms of DPI systems, Voss and Finley (5) studied the performance of a carrier system (Ventolin™ GSK) containing salbutamol sulphate and using a custom de-agglomeration rig. In this study, they concluded that while turbulence played an important role, it was not the only mechanism of de-aggregation in carrier-based systems. In 2004, the same group used an impinging jet to study the dispersion of the same carrier formulation and reported that the jet velocity and total powder dose influenced aeosolisation efficiency (6). In 2006, Louey *et al.* (7) developed a series of standardized entrainment tubes ranging from 4.5 mm to 11 mm in diameter. Utilising a Ventolin™ carrier-based formulation, they reported good correlation between flow rate, Reynolds number (ranging between 3,644–18,443) and aerosolisation efficiency.

These previous studies utilized horizontally mounted entrainment tubes (which have the gravitational force perpendicular to the air flow). In 2008, Kurkela *et al.* (8) developed a vertically mounted de-agglomeration apparatus utilising turbulent flow and found the Reynolds number (ranging from 7,000–46,000) to be related to the aerosol performance of a model carrier system (containing 138 μm borosilicare glass carrier particles with 2.5μm silica fines). However, this vertical design was not used to study 'real' pharmaceutical systems or agglomerate-based formulations.

Interestingly, the aforementioned research tested carrier-based formulations (which consist of small drug particles blended on much larger carrier particles) rather than agglomerated systems. Recently, Gac *et al.* (9) attempted to simulate the aerosolisation of a small powder bed (93 particles), analogous to a drug-only agglomerate, in turbulent air streams using an eddy fluid particle model, which solves for the flow using an inviscid approach. In this study, they tried to correlate computational results with experimental measurements made using a horizontal entrainment tube with turbulence promoters. They found that turbulence resulted in the de-agglomeration of di-sodium cromoglycate API; however, the nature of the initial powder (in terms of agglomeration) was not tightly controlled, and the degree of impaction due to localized turbulent eddies near the powder induction port was not studied. Many other de-agglomeration rigs have been used to study the phenomena of particle de-agglomeration, and the excellent review by Calvert *et al.* (4) reports the different approaches used, the limitations of the apparatuses and the findings of each study. One thing is clear, however, the exact mechanism underlying particle de-agglomeration is not fully understood, and the parameters that affect one system (i.e. carrier-based formulations) may not be applicable to another system (i.e. agglomerated fine powders). Furthermore, complex variables, such as size distribution, particle shape, surface energy and environmental conditions, will play a significant role, and these must be taken into account when predicting powder behaviour.

Recently, with the advance of easily accessible, high-speed computing facilities, computational approaches are being applied to solve the problem of particle fluidization and de-agglomeration. For example, Gac *et al.* (9) utilised an eddy fluid particle model coupled with a molecular dynamics-like model to predict particle fluidisation in a two-dimensional flow field. Discrete element modelling (DEM) has begun to find a niche within the area of particle de-agglomeration (10,11), where the interactions and velocities of particles or agglomerates may be predicted as a function of time. It is important to note, however, that this technique is generally *in vacuum* (i.e., it does not take into account the fluid flow) and is computationally expensive, especially when each agglomerate contains over 100,000 particles in the micron size range. Also, limited studies exist focussed on using DEM in pharmaceutical aerosol science, and the studies reported previously generally focus on larger particulate structures (where primary particles range from 10 μm–1,000 μm). Some studies have focussed on particles within the size range applicable for inhalation science (12,13), with the recent one by Iimura *et al.* showing how an applied shear force to powder beds (containing 500, 500 nm particles) could be used to simulate powder entrainment (13). Eventually, the coupling of computational fluid dynamics (CFD) methodology to DEM may provide a means to predict the aerosolisation process as a whole. At the present, the computational cost and coupling methodology mean this has been limited to small numbers of large particles (usually within the areas of granular and fluidized bed flow) (14,15).

Computational fluid dynamics is an established methodology for the prediction of fluid flow and has been used to predict the properties of flow in the respiratory tract (16–18) and in devices used for inhalation (16,19–23). Information gleaned from CFD may be directly applied to the fate of particulate systems in DPIs and the lung. For example, Coates *et al.* demonstrated how CFD modelling of DPI mouthpiece geometry (23), dispersion grid (21), air inlet size (19), air flow rate (16) and capsule properties (20) could be used to investigate aerosol performance, comparing the results with *in vitro* experimental measurements. Whilst the results of these studies gave insight into DPI aerosolisation, de-convolution of the physical mechanisms taking place was difficult due to the multi-variable nature of conventional DPIs.

To study the aerosolisation and de-agglomeration process at a fundamental level, each variable (for example

turbulence or impaction) should be studied discretely. Furthermore, limited information is available in the literature focused on the experimental break-up of agglomerate-based formulations. This study aims to investigate a model pharmaceutical agglomerate system, with a focus on elucidating the mechanism underlying powder break-up and aerosolisation. By combining CFD with conventional experimental entrainment tubes (constructed using three-dimensional printing to eliminate engineering constraints encountered in previous studies) we aim to investigate each variable in turn. This paper focuses on the influence of venturi-driven turbulence effects on agglomerate break-up.

MATERIALS AND METHODS

Materials

Spray-dried mannitol (batch number M08-060) was supplied by Pharmaxis Ltd. (Sydney, Australia). Water was purified by reverse Osmosis (MilliQ, Molsheim, France). All solvents were analytical grade and were supplied by Sigma (Sydney, NSW, Australia).

Preparation of a Model Particulate System

In order to evaluate the influence of venturi effects on particle dispersion and aerosolisation, a model agglomerate system was prepared. Since micron-sized material tends to self-agglomerate, to minimize variability in agglomerate size, mannitol was subjected to Turbula mixing (Bachofen AG Maschinenfabrik, Basel, Switzerland) in a cylindrical aluminium container (25 mm diameter × 36 mm length) at 42 rpm for 15 min using conditions reported previously (24). After mixing, the primary agglomerates were passed through a nest of sieves (ISO 3310-1 test sieves, Endecotts Ltd., London, UK) to produce a 500 μm–800 μm sieve fraction. The agglomerated powders were stored in sealed containers at 45% RH and 25°C for a minimum of 48 h prior to their use.

Physical and Chemical Characterisation

The primary mannitol particle size distribution was measured by laser diffraction (Malvern Mastersizer 2000, Malvern, Worcestershire, UK). Samples were dispersed in chloroform and sonicated for 5 min prior to analysis. An aliquot of the suspension was then transferred to the small dispersion cell of the Malvern particle sizer until obscuration between 15% and 30% was achieved. Particle size was measured using a refractive index of 1.52 for mannitol and 1.44 for chloroform. Samples were measured in triplicate. The particle size of the agglomerates was measured using optical microscopy (CX41 microscope with DP12 digital camera, Olympus, Japan). Briefly, samples were dispersed on a glass slide, and images were recorded using the associated CCD camera and image capture software. Wide field images were collected and exported to the Image-J software (National Institute of Mental Health, Maryland, USA). Images were processed by threshold analysis to produce particle area and diameter parameters. Approximately 300 particles were analysed. The mass of 25 agglomerates was measured individually using a Seven Figure Cahn microbalance at 45% RH and 25°C (DVS-1, Surface Measurement Systems Ltd., London, UK).

The surface area of the primary mannitol particles was investigated using nitrogen adsorption at 77K (Tristar II 3020, Micromeritics, Norcross, GA, USA). Samples (ca. 0.3 g) were accurately weighed into standard glass bulbs and dried under nitrogen at 40°C for 24 h prior to analysis (VacPrep 061, Micromeritics). The sample was analysed in triplicate. The true density of the primary mannitol particles was measured using helium pycnometry (Accupyc 1340 Gas Pycnometer, Micromeritics). Samples (ca. 30 g) were prepared using the same method as for the surface area measurements. During each analysis the temperature was maintained at 27°C, and ten repeat analyses were performed on the sample.

The concentration of mannitol in aqueous samples was measured using high performance liquid chromatography (HPLC). A LC20AT pump, SIL20AHT autosampler, CBM-Lite system controller with a pc-computer running LC solution v1.22 software and a RID-10A refractive index detector (Shimadzu, Sydney, NSW, Australia) were utilised. An 8 mm Resolve C18 Radial Pack chromatography Cartridge (Waters Asia Ltd., Singapore) was used for separation at a flow rate of 1 $mL.min^{-1}$. Purified water was used as the mobile phase.

Construction of Entrainment Venturi Tubes

A series of venturi tubes was constructed from acrylonitrile butadiene styrene (ABS) using a rapid-prototype three-dimensional printer (Dimension Elite, Dimension Inc., Eden Prairie, MN, USA) and computer-aided design software (ANSYS Design Modeler v11.0; ANSYS, Canonsburg, PA, USA). The tubes were constructed of 290 mm long interlocking sections with a core diameter of 19 mm and a final 279.5 mm venturi section. When assembled, the total tube length was 2.20 m, with the final exit tube tapering to 19 mm (straight tube), 16 mm, 13 mm or 10 mm in diameter over a 50 mm length (see Fig. 1). The reduction in tube diameter at the exit point acted as a venturi, inducing a localised increase in velocity and turbulence intensity (exit velocities and Reynolds numbers (Re) for flow rates between 15 and 140 $L.min^{-1}$ are given in Fig. 2). From Fig. 2, it can be seen

that the venturi tubes were constructed so that flow was laminar at 15 L.min^{-1} (Re < 3000) and turbulent at all other flow rates.

Aerosol Characterisation

The break-up of mannitol agglomerates and aerosolisation process in the four venturi tubes, as a function of flow rate, was measured using laser diffraction. Each tube was mounted vertically on a secure scaffold assembly with the venturi exit connected in-line to a Spraytec particle sizer (Malvern Instruments, Malvern, UK). A Gast Rotary vain pump (Erweka GmbH, Heusenstamm, Germany) was connected to the outlet of the particle sizer, and the flow was calibrated using a flow meter (TSI 3063, TSI instruments Ltd., Buckinghamshire, UK). For each measurement, 50 mg of the agglomerated powder was introduced into the centre of the airstream at the top of the assembly using a funnel. The size at the exit point of the venturi was measured in real-time using the Spraytec software at 2,500 sweeps per second (range 0.1 μm–2,000 μm). After each experimental protocol, the data set was processed to produce an average particle size distribution, as well as 10% ($d_{0.1}$), 50% ($d_{0.5}$) and 90% ($d_{0.9}$) percentile undersize, geometric standard deviation (GSD), span and percentage of particles with a diameter <5 μm (equivalent to the fine particle fraction).

Two variables (flow rate and venturi diameter) were tested with four parameters for diameter (19 mm, 16 mm, 13 mm and 10 mm) and four parameters for flow rate (15, 60, 100 and 140 L.min^{-1}). In addition, a flow rate of 0 L.min^{-1}, which corresponded to gravitational acceleration, was studied as a control. All measurements were conducted in triplicate.

Wall deposition of mannitol in the different venturi tubes was investigated at the upper and lower flow rates, to study potential wall collision. Briefly, the venturi section was

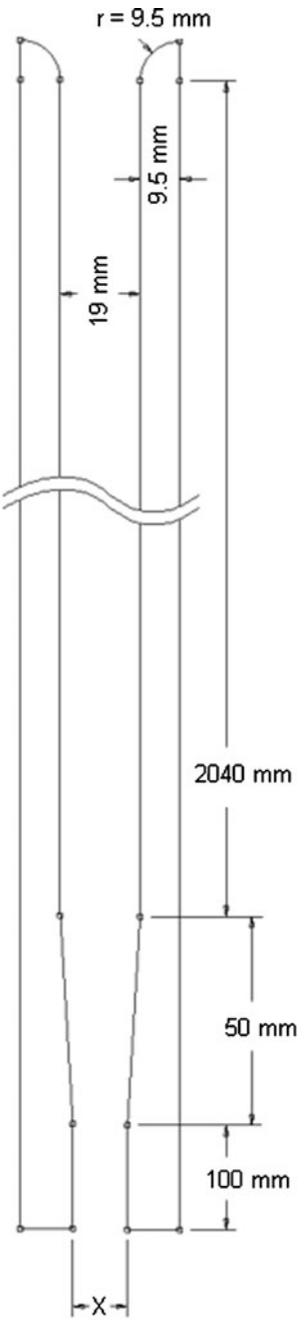

Fig. 1 Schematic of the venturi tubes (X = 19 mm, 16 mm, 13 mm or 10 mm).

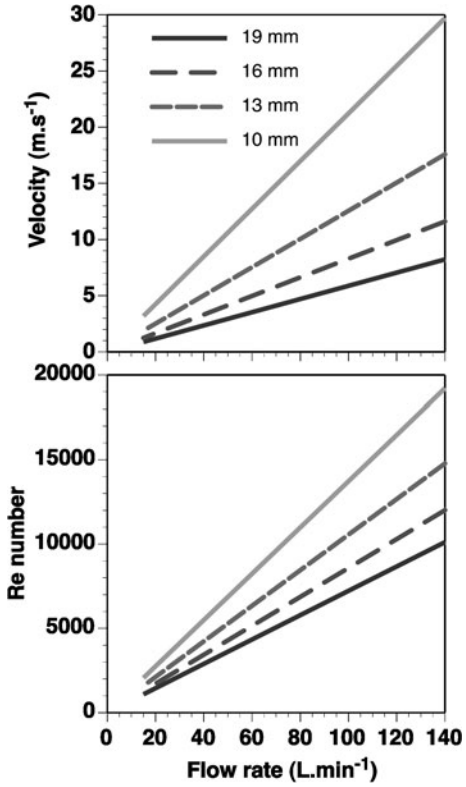

Fig. 2 Exit velocity and Reynolds number for different venturi tubes (legend indicates exit tube diameter).

disassembled and washed with 5 mL purified water and was analysed using HPLC.

Computational Fluid Dynamic Analysis

A commercially available computational fluid dynamics code, ANSYS CFX v11 (ANSYS, Canonsburg, PA, USA) was used to simulate the flow of air through the venturi tubes, to predict turbulence properties and to track particles through the gas flow. The fluid utilised was air at 25°C (which was assumed to be incompressible at low flow velocities), and the flow fields were resolved by solving the Reynolds-averaged Navier Stokes equations using a finite volume method based on a tetrahedral mesh with inflation at walls to capture the boundary layer behaviour correctly. Turbulence was modelled using the shear stress transport model (25) with scalable wall functions.

In addition, Lagrangian particle tracking was conducted via post-processing, as the particle concentration was too low to affect the flow field. Solid spherical particles were utilised to represent each agglomerate. The size distribution of these solid spherical particles was set to be equivalent to the size distribution of the agglomerates, and a density equivalent to the packing density of the agglomerates (as outlined in the following sections) was utilised. Particle wall impactions were calculated by setting the venturi walls to have a zero coefficient of restitution and introducing a fixed number of particles with a given size and density at the inlet port of the venturi tube. A mesh independence analysis was conducted to ensure the computational results were independent of mesh size. This was achieved by studying the axial velocity profiles as a function of increasing mesh density. Mesh independence was confirmed when the mesh size contained 1.6×10^5 nodes. A higher resolution mesh (containing 2.5×10^5 nodes) was utilised for computational analysis.

Statistical Analysis

Data were subjected to statistical analysis using the SPSS Statistics 17.0 software package (SPSS Inc, Chicago, Illinois, USA). One-way ANOVA analysis (with Tukey's post hoc analysis) was utilised to test for significance. A difference was considered significant when $p<0.05$.

RESULTS AND DISCUSSION

Physical Characterisation of the Primary Mannitol Particles

The accurate determination of the physical properties of the primary mannitol particles is critical to this study, since particle diameter, surface area and true density are used to calculate theoretical values for the agglomerate structure. Analysis of the size distribution of the primary manitiol particles, using laser diffraction, indicated 90% of the particles had a volume diameter $\leq$ 6.82 μm±0.37 μm and 10%≤1.95 μm±0.02 μm. The median $d_{0.5}$ particle diameter of the primary particles was 3.91 μm±0.15 μm. This value was used for theoretical calculation of the agglomerate structure. The true density of the primary mannitol particles, measured by helium pycnometry, was 1,435.2±0.6 $kg.m^{-3}$, which is in good agreement with values published previously (~1,450–1,520 $kg.m^{-3}$ (26)). The surface area of the primary mannitol particles, measured by nitrogen adsorption and calculated using the BET method, was 2.6057±0.0259 $m^2.g^{-1}$.

Characterisation of the Mannitol Agglomerates

The particle size distribution of the mannitol agglomerates, measured by optical microscopy, is shown in Fig. 3. Linear regression of the particle size distribution over a 5–95% cumulative percentage suggested a normal distribution ($R^2=0.993$) with 90% of particles having a diameter <759.9 μm and 10% of particles having a diameter <525.6 μm. Such observations are in good agreement with the sieve sizes used (500–800 μm). The median particle diameter of the agglomerate system was 642.8 μm. The normal distribution and linear regression equation were used to model the size distribution, *in silico*, for CFD particle tracking measurements.

Analysis of the agglomerate microbalance data indicated a mean mass of 91.1 μg±22.1 μg, suggesting that based on the 50 mg sample size, approximately 550 agglomerates would be entrained into the air stream. Furthermore, based on the measured median agglomerate diameter and mean mass values, a theoretical agglomerate sphere density may be calculated. A density of 786 $kg.m^{-3}$ was calculated;

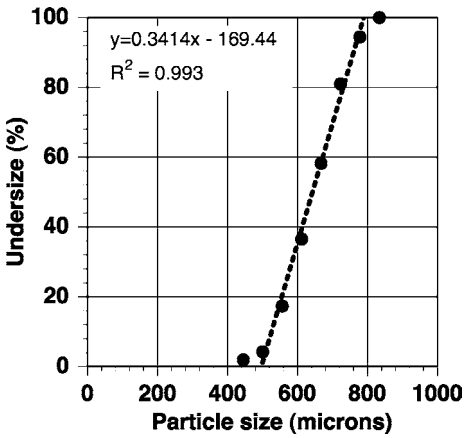

Fig. 3 Size distributions of the model agglomerate system.

however, it is important to note that this theoretical value is based on the assumption of perfect spherical particles with equivalent packing density across the agglomerate size range used.

Using the true density value for the primary mannitol particles of 1,435 kg.m^{-3}, an agglomerate packing density ratio of 0.46 was calculated. Such observations are less than the theoretical maximum value of 0.64 for the packing density of close-packed spheres (27), but are greater than for simulations of 1 μm (packing density ratio of 0.21) and 5 μm (packing density ratio of 0.35) spheres predicted using discrete element modelling of 10,000 particles under centripetal motion (12). Presumably the variation is due to the lognormal distribution of the primary particles and the number of particles involved. Using the median single particle diameter of 3.91 μm and density of 1435 kg.m^{-1}, we can predict that each agglomerate contains approximately two-million particles.

Computational Fluid Dynamics Analysis

The venturi tube assembly was 2.20 m in length to ensure a fully developed flow prior to entry into the 50 mm venturi section. Axial velocity and turbulence kinetic energy at 140 L.min^{-1} were plotted as a function of axial distance along the tube at 50 mm, 150 mm, 200 mm, 500 mm and 2200 mm points along the assembly (which is the equivalent of approximately 3 diameters (D), 8D, 11D, 27D and 116D, respectively) and are shown in Fig. 4A and B, respectively. Fig. 4A shows that at 140 L.min^{-1} a fully developed flow profile is achieved at 1,000 mm, as there is no change in the axial velocity until the airstream reached the venturi section (data at 2,160 mm). Similar observations were made for the other flow rates (data not shown). In addition, it can be seen that the axial velocity profile across the diameter of the tube remains relatively constant with a steep decrease to zero velocity at the tube walls. Fig. 4B shows the turbulence kinetic energy as a function of axial position (at the same axial locations as used for the velocity analysis). In general, higher turbulence values were observed in the boundary layer with a decrease towards the axis of the venturi assembly.

Previous studies by Coates *et al.* (19) calculated that for a standard Aerolizer™ DPI (Plastiape S.p.A, Osnago, Italy) operating at a flow rate of 60 L.min^{-1}, a volume-averaged velocity of 14.1 m.s^{-1} was observed (exit velocity: 11.9 m.s^{-1}) with a volume-averaged integral scale strain rate of 5,110 s^{-1} (ISSR, defined as the turbulence eddy dissipation rate divided by the turbulence kinetic energy). These values are similar to those observed in the venturi tubes studied here, where the ISSR varied from the 4,049 s^{-1} to 4,759 s^{-1}, and the exit velocity varied from 13.0 m.s^{-1} to 30.2 m.s^{-1} between 60 L.min^{-1} and 140 L.min^{-1} flow rates, respectively. In another study, Coates *et al.* (16) reported volume-averaged turbulence kinetic energy values of 6 m^2.s^{-2} at 60 L.min^{-1} in the Aerolizer™ DPI. In comparison, analysis of the venturi tubes gave volume-averaged turbulence kinetic energy values of 0.26–1.39 m^2.s^{-2} between 60 L.min^{-1} and 140 L.min^{-1}, respectively (similar to the values for the Aerolizer™ at 30 L.min^{-1}, 0.8 m^2.s^{-2} (16)). It is important to note, however, that it is difficult to compare the volume-averaged values, since the venturi tubes used in this study are much larger in size, and localised values for turbulence kinetic energy regularly exceeded the mean values reported previously.

Particle tracking measurements for all flow rates and venturi diameters were calculated for 500–5,000 particles (in order to ensure no statistical variation due to the number of particles processed) with a median diameter 525.6 μm (with a normal distribution as described in Fig. 3) and density of 786 kg.m^{-3}. This size distribution and density were based on the measured particle system used in the study. In general, most particles impacted on or in close proximity to where the tube narrows, and the number of impactions increased with flow rate and decreased with venturi diameter. For example, the number of impactions in the 19 mm tube varied from 2.18% to 14.00% between 60 L.min^{-1} and 140 L.min^{-1}. In comparison, impactions in the 10 mm venturi tube varied from 45.09% to 59.27% at 140 L.min^{-1}. In addition, impact angles and impact velocities of particles on the walls of the venturi section were output from CFX from which normal impact velocities were calculated.

Particle tracking for tubes with venturi diameters of 16 mm–10 mm resulted in a distinct bimodal distribution of impacting particles, with a group impacting at angles exceeding 1.5° and another at angles below 0.5°. In these cases, particles with impact angles less than 0.5° were excluded, as these particles had similar normal impact velocities and impact angles to particles in the 19 mm straight tube, which displayed negligible particle break-up. In general, normal velocities ranged from 0.02–0.87 m.s^{-1} and increased with airflow and reduction in venturi diameter.

Particle Aerosolisation

The particle size of the model agglomerates after they had passed through the venturi assemblies at different flow rates was measured using laser diffraction. In order to evaluate the influence of flow and venturi exit diameter on agglomerate break-up, the percentile volume diameter (d_x) and percentage of particles with a diameter < 10 μm and <5 μm were calculated. At a flow rate of 0 L.min^{-1} (gravitational sedimentation), there were no particles <10 μm detected for all venturi tubes, suggesting that no

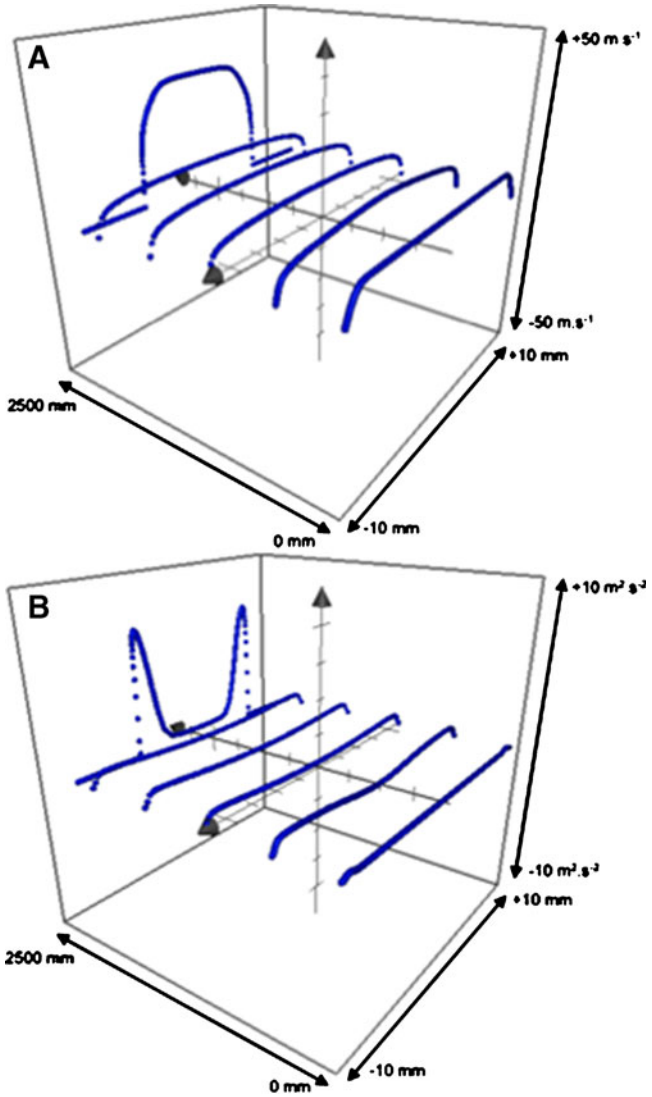

Fig. 4 (**A**) Velocity and (**B**) turbulence kinetic energy along the length of the 10 mm venturi assembly at 140 L.min^{-1} (where 50 mm represents the assembly inlet and 2200 mm represents the venturi outlet).

agglomerate break-up occurred. Similar results were observed for the 15 L.min^{-1} laminar flow studies. Furthermore, no significant differences were observed between the $d_{0.5}$ or $d_{0.1}$ as a function of venturi diameter at either flow rate.

In comparison, analysis of the particle size distributions at flow rates $\geq$ 60 L.min^{-1} indicated venturi-dependent size distributions. For example, no significant increase in the percentage particles < 10 μm was observed for the 19 mm tube until a flow rate of 140 L.min^{-1} was obtained (1.41% ±0.36%), while a flow rate of 60 L.min^{-1} was sufficient to induce agglomerate break-up in the 10 mm venturi. The effect of flow rate on the particle size distribution in the 10 mm venturi is shown in Fig. 5. As seen in Fig. 5, at 0 L.min^{-1} and 15 L.min^{-1}, a mono-modal size distribution was observed (equivalent to the primary agglomerate size). As the flow was increased above 60 L.min^{-1} a multi-modal size distribution was observed, with an increase in the volume of particles that approached the primary particle size distribution (see Fig. 5B). It is interesting to note, however, that the size distribution of the de-agglomerated particles was bigger than that of the primary mannitol size (where 90% of primary particles <7 μm, in comparison with 90%~ < 20 μm). Such observations suggest that the detached/de-agglomerate particles were in the form of multiplet or micro-agglomerates.

Relationship Between Computational and Experimental Measurements

Clearly, an increase in the axial velocity and a decrease in the venturi diameter results in an increase in agglomerate break-up; however, it is not clear whether this is due to turbulence or impaction. To evaluate the break-up mechanism, each variable should be studied with relationship to the particle size distribution. Subsequently, the $d_{0.1}$ was chosen as the descriptor of the degree of agglomerate break-up and was compared with velocity, turbulence and

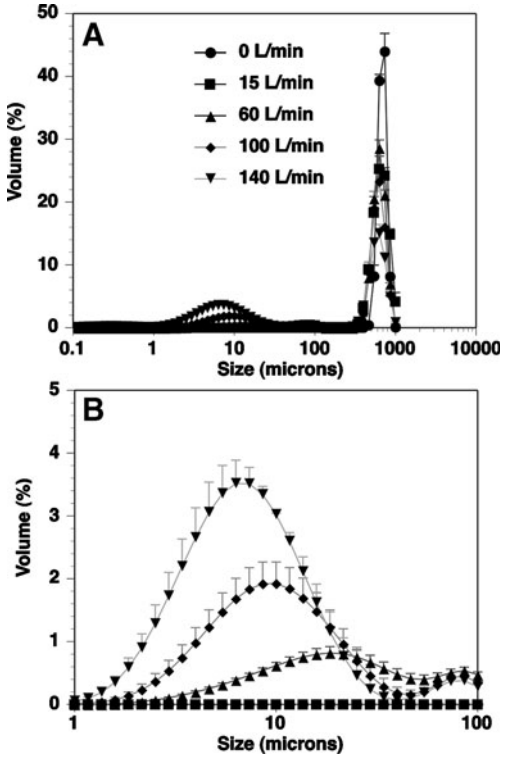

Fig. 5 Effect of airflow rate on the particle distribution in the 10 mm venturi tube measured via laser diffraction. (**A**) Full distribution profile; (**B**) magnification of fine particle size data. Error bars indicate standard deviations of three measurements.

impaction factors (other descriptors were also studied, including %< 10 μm, % <5 μm; however, these showed similar results and are not reported here).

The focus of this project was to study the influence of venturi-induced turbulence on agglomerate break-up. Consequently, the apparatus was designed to ensure a fully developed flow, with minimised impaction. Fig. 6 is a plot of the $d_{0.1}$ versus the Reynolds number for all tubes and velocities. As discussed, the Reynolds numbers in the venturi ranged from ~1,000 to 20,000, with all tubes exhibiting laminar flow at the lowest flow rate (15 L.min^{-1}) and turbulent flow at all other flow rates (≥ 60 L.min^{-1}). Analysis of the $d_{0.1}$ for all datasets over this range showed no relationship. For example, at a Reynolds number of 8,570, the 10 mm venturi produced a $d_{0.1}$ of 52.5 μm± 19.7 μm, yet at a Reynolds number of 12,000, the 16 mm tube produced a $d_{0.1}$ of 429.1 μm±14.8 μm. In addition to the Reynolds number, the volume-averaged turbulence kinetic energy, average turbulence eddy frequency, turbulence length-scale, ISSR and pressure drop across the venturi were evaluated in terms of the $d_{0.1}$ and showed no direct relationship.

The lack of relationship between turbulence factors and particle size distribution is interesting, since previous studies have suggested turbulence to be a dominating factor in particle aerosolisation (8,10,12,20). Factors such as pressure drop affecting performance have also been reported by Mendes *et al.* (28) (where the DPI devices tested had pressure drops ranging from 0.2 kPa to 1.6 kPa resulting in FPFs ranging from ~15% up to ~30%); however, this study again shows no direct relationship between pressure drop and aerosol performance (for example, a pressure drops of 0.9 kPa was calculated in the 10 mm venturi). Furthermore, the aerosol performance was much lower than those reported by Mendes *et al.* (28). Apart from the work by Coates *et al.* (6,19–21,23), the focus in these previous studies was mainly on carrier-based systems, which may have a different mechanism of powder entrainment and aerosolisation, since their performance is governed by the removal of small particles from large carrier surfaces rather than the break-up of a large agglomerate containing many similarly sized particulates.

Although particle impaction was limited in this study (since the focus was on turbulence effects), significant wall impactions were predicted computationally, with increased flow rate and reduced venturi diameter. Consequently, it may be suggested that impaction plays a dominant role in this system. To analyse such a hypothesis, the deposition of mannitol on the internal walls of the venturi tube at 15 L.min^{-1} and 140 L.min^{-1} was studied. For the straight tube (19 mm), an increase in flow rate from 15 L.min^{-1} to 140 L.min^{-1} resulted in a statistically significant increase in wall deposition from 0.143 mg±0.020 mg to 0.277 mg± 0.059 mg. Interestingly, there was no significant difference between mannitol wall deposition at 15 L.min^{-1} and at 0 L.min^{-1} (0.131 mg±0.011 mg under gravitational sedimentation), suggesting laminar flow did not induce particle wall collision. Analysis of mannitol deposition in the 10 mm diameter venturi indicated higher agglomerate wall

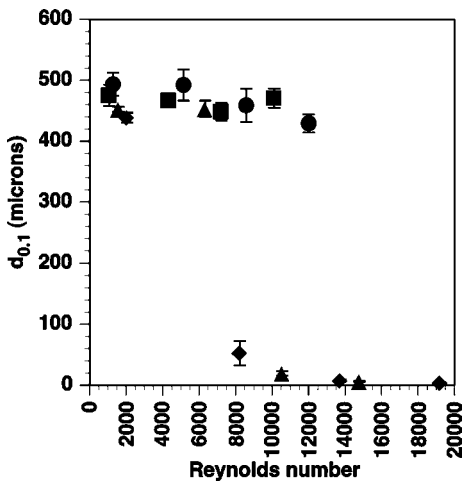

Fig. 6 Effect of the Reynolds number on the particle $d_{0.1}$ for all venturi tubes (■:19 mm, ●:16 mm, ▲:13 mm, ◆:10 mm).

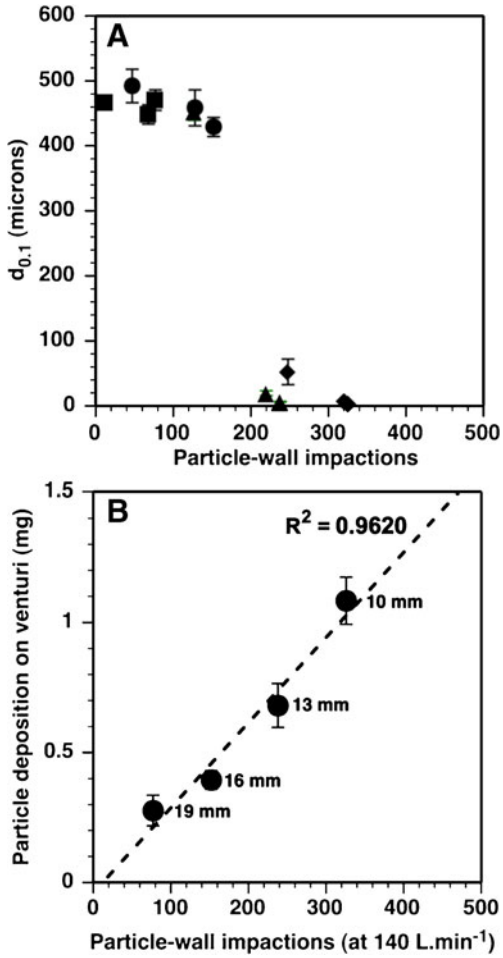

Fig. 7 (**A**) Relationship between $d_{0.1}$ and the calculated number of particle-wall impactions at all flow rates (■:19 mm, ●:16 mm, ▲:13 mm, ◆:10 mm). (**B**) Relationship between drug mass deposited in the venturi tube at 140 L.min^{-1} and the calculated number of particle-wall impactions.

interaction, with a significant increase from 0.528 mg± 0.013 mg to 1.083 mg±0.091 mg between 15 L.min^{-1} and at 140 L.min^{-1}, respectively. In addition, a relatively small but statistically significant increase in deposition was seen in the gravitational settling case (0.601 mg±0.012 mg) compared with the 15 L.min^{-1} data. Such observations are to be expected, since the gravitational sedimentation would likely encounter increased random contact with the walls in the tubes with greater tapering.

To visualise the relationship between particle deposition, flow and venturi diameter, the $d_{0.1}$ was plotted as a function of computed number of wall collisions (Fig. 7A). Analysis of the data showed that a critical percentage of particles impacting of ~20% was required prior to successful break-up, which suggests that there was a relationship between the number of particle impacts and the $d_{0.1}$. However, it is important to note that this correlation is likely to be dependent on factors such as the velocity magnitude and direction rather than simply the number of impactions. Interestingly, no relationship between number of impactions and Re was found. This is to be expected, however, since no relationship between turbulence factors and particle break-up was observed when analysing particle size distribution data.

To further study the relationship between particle impaction and aerosol de-agglomeration, the percentage of the mannitol deposited on the wall of the experimental venturi tubes (based on a 50 mg sample mass) was analysed and compared with the number of impactions calculated *in silico* (Fig. 7B). Analysis of these data suggests a direct linear correlation between the theoretically calculated number of collisions and the total recovered drug content (R^2=0.9620), suggesting that the number and speed of impactions were increasing with increasing flow rate and reduced venturi diameter.

To further study if impaction was the driving force for particle break-up, the impact angle and velocities were calculated using CFD, and the normal impact velocities were plotted as a function of $d_{0.1}$. The impact angle of the particles was within the same range as the angle of the venturi (namely 1.7°, 3.4° and 5.1°, for the 16 mm, 13 mm and 10 mm tubes, respectively). In general, the normal impact velocity ranged between 0.01 m.s^{-1} and 1 m.s^{-1}, and no change in $d_{0.1}$ was observed until a velocity of approximately 0.4 m.s^{-1} was achieved (Fig. 8). This observation seems to be in agreement with previous studies using DEM, which have suggested a critical velocity is required to result in agglomerate fragmentation and break-up (29,30); however, the size distribution and particle number in these DEM studies were not equivalent and, thus, cannot be extrapolated to the critical velocity reported in this study.

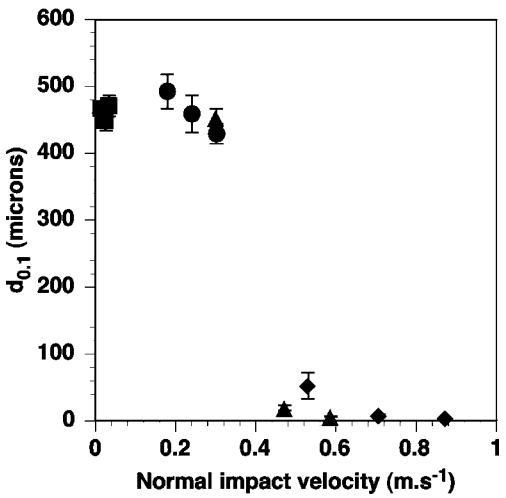

Fig. 8 Relationship between $d_{0.1}$ and the calculated normal impact velocities at all flow rates for all venturi tubes rates (■:19 mm, ●:16 mm, ▲:13 mm, ◆:10 mm).

Interestingly, particle size distributions in tubes which display agglomerate break-up took on a distinctly bimodal shape (Fig. 5). If agglomerates impacted on the surface of the tube and underwent major fragmentation, it would be expected that the second mode (~700 μm) would broaden due to fragments being emitted from the tube. However, a broadening in this mode was not observed, suggesting that at highly acute impact angles (1.7°–5.1°), primary particles are detached without significant fracture of the main agglomerate.

CONCLUSIONS

This study focussed on the influence of venturi-created turbulence effects on the aerosolisation and break-up of pharmaceutical agglomerates for inhalation. While the venturi tubes were designed to minimise other potential powder de-agglomeration mechanisms, it appears that for agglomerated inhalation powders, particle-wall impaction played a dominating role. The design and evaluation of an impaction rig to study aspects such as impact velocity and angle on this model system will be considered in further studies.

ACKNOWLEDGEMENTS

This research was supported under the Australian Research Council's Linkage Projects funding scheme (project LP0776892). The views expressed herein are those of the authors and are not necessarily those of the Australian Research Council.

REFERENCES

1. Smith IJ, Parry-Billings M. The inhalers of the future? A review of dry powder devices on the market today. Pulm Pharmacol Ther. 2003;16(2):79–95.
2. Newman SP, Busse WW. Evolution of dry powder inhaler design, formulation, and performance. Resp Med. 2002;96(5):293–304.
3. Islam N, Gladki E. Dry powder inhalers (DPIs)—A review of device reliability and innovation. Int J Pharm. 2008;360(1–2):1–11.
4. Calvert G, Ghadiri M, Tweedie R. Aerodynamic dispersion of cohesive powders: A review of understanding and technology. Adv Powder Technol. 2009;20(1):4–16.
5. Voss A, Finlay WH. Deagglomeration of dry powder pharmaceutical aerosols. Int J Pharm. 2002;248(1–2):39–50.
6. Wang ZL, Lange CF, Finlay WH. Use of an impinging jet for dispersion of dry powder inhalation aerosols. Int J Pharm. 2004;275(1–2):123–31.
7. Louey MD, Van Oort M, Hickey AJ. Standardized entrainment tubes for the evaluation of pharmaceutical dry powder dispersion. J Aerosol Sci. 2006;37(11):1520–31.
8. Kurkela JA, Brown DP, Raula J, Kauppinen EI. New apparatus for studying powder deagglomeration. Powder Technol. 2008;180 (1–2):164–71.
9. Gac J, Sosnowski TR, Gradon L. Turbulent flow energy for aerosolization of powder particles. J Aerosol Sci. 2008;39(2):113–26.
10. Thornton C, Liu LF. How do agglomerates break? Powder Technol. 2004;143–4:110–6.
11. Moreno R, Ghadiri M, Antony SJ. Effect of the impact angle on the breakage of agglomerates: a numerical study using DEM. Powder Technol. 2003;130(1–3):132–7.
12. Yang RY, Yu AB, Choi SK, Coates MS, Chan HK. Agglomeration of fine particles subjected to centripetal compaction. Powder Technol. 2008;184(1):122–9.
13. Iimura K, Watanabe S, Suzuki M, Hirota M, Higashitani K. Simulation of entrainment of agglomerates from plate surfaces by shear flows. Chem Eng Sci. 2009;64(7):1455–61.
14. Guo Y, Kafui KD, Wu CY, Thornton C, Seville JPK. A coupled DEM/CFD analysis of the effect of air on powder flow during die filling. AIChE J. 2009;55(1):49–62.
15. Kloss C, Kahrimanovic D, Pirker S, editors. Coupling of DEM and CFD—Simulation and experiment. DANSIS Meeting on Discrete Element Methods; 2009; Kopenhagen.
16. Coates MS, Chan HK, Fletcher DF, Raper JA. Influence of air flow on the performance of a dry powder inhaler using computational and experimental analyses. Pharm Res. 2005;22(9):1445–53.
17. Longest PW, Vinchurkar S. Validating CFD predictions of respiratory aerosol deposition: Effects of upstream transition and turbulence. J Biomech. 2007;40(2):305–16.
18. Ma B, Lutchen K. CFD simulation of aerosol deposition in an anatomically based human large-medium airway model. Ann Biomed Eng. 2009;37(2):271–85.
19. Coates MS, Chan HK, Fletcher DF, Raper JA. Effect of design on the performance of a dry powder inhaler using computational fluid dynamics. Part 2: Air inlet size. J Pharm Sci. 2006;95 (6):1382–92.
20. Coates MS, Fletcher DF, Chan HK, Raper JA. The role of capsule on the performance of a dry powder inhaler using computational and experimental analyses. Pharm Res. 2005;22 (6):923–32.
21. Coates MS, Fletcher DF, Chan HK, Raper JA. Effect of design on the performance of a dry powder inhaler using computational fluid dynamics. Part 1: Grid structure and mouthpiece length. J Pharm Sci. 2004;93(11):2863–76.
22. Longest PW, Hindle M. Evaluation of the respimat soft mist inhaler using a concurrent CFD and *in vitro* approach. J Aerosol Med Pulm D. 2009;22(2):99–112.
23. Coates MS, Chan HK, Fletcher DF, Chiou H. Influence of mouthpiece geometry on the aerosol delivery performance of a dry powder inhaler. Pharm Res. 2007;24(8):1450–6.
24. Adi H, Kwok P, Crapper J, Young PM, Traini D, Chan HK. Does electrostatic charge affect powder aerosolisation? J Pharm Sci. 2009;Accepted 18th Sept 2009.
25. Menter FR. 2-equation eddy-viscosity turbulence models for engineering applications. AIAA J. 1994;32(8):1598–605.
26. Chew NY, Chan HK. Influence of particle size, air flow, and inhaler device on the dispersion of mannitol powders as aerosols. Pharm Res. 1999;16(7):1098–103.
27. Jaeger HM, Nagel SR. Physics of the granular state. Science. 1992;255(5051):1523–31.
28. Mendes PJ, Pinto JF, Sousa JMM. Non-dimensional functional relationship for the fine particle fraction produced by dry powder inhalers. J Aerosol Sci. 2007;38(6):612–24.
29. Thornton C, Yin KK, Adams MJ. Numerical simulation of the impact fracture and fragmentation of agglomerates. J Phys D Appl Phys. 1996;29(2):424–35.
30. Subero J, Ning Z, Ghadiri M, Thornton C. Effect of interface energy on the impact strength of agglomerates. Powder Technol. 1999;105(1–3):66–73.